Research Article Vol. 62, No. 10 / 1 April 2023 / Applied Optics 2629

applied optics

Far ultraviolet mirrors for aurora imaging: design and fabrication

Xiaodong Wang,* Peng Zhou, Shuai Ren, Xinkai Li, Haifeng Wang, Xin Zheng, and Bo Chen

Changchun Institute of Optics, Fine Mechanics and Physics, Chinese Academy of Sciences, Changchun 130033, China
**wangxiaodong@ciomp.ac.cn*

Received 24 January 2023; revised 3 March 2023; accepted 5 March 2023; posted 6 March 2023; published 24 March 2023

The emission lines of 140–180 nm are auroral bands of N_2 Lyman–Birge–Hopfield, and they have been imaging targets of many satellites that need reflective mirrors. To obtain good imaging quality, the mirrors also should have excellent out-of-band reflection suppression as well as high reflectance at working wavelengths. We designed and fabricated non-periodic multilayer LaF_3/MgF_2 mirrors with working wave bands of 140–160 nm and 160–180 nm, respectively. We used a match design method and deep search method to design the multilayer. Our work has been utilized in the new wide-field auroral imager of China, and the application of these notch mirrors with excellent out-of-band suppression reduces the utilization of corresponding transmissive filters in the optical system of space payload. Furthermore, our work provides new routes for the design of other reflective mirrors in the far ultraviolet region.

https://doi.org/10.1364/AO.482763

1. INTRODUCTION

The aurora is generated by collisions between energetic charged particles and atmospheric gases (N_2 and O_2) at high altitude. Imaging of the aurora from space provides spatial/temporal information that maps back to different regions of the magnetosphere [1–3]. The emission lines of 140–180 nm are auroral bands of N_2 Lyman–Birge–Hopfield (LBH). Wave bands of 140–160 nm are referred to as LBH-short (LBH-S), and those of 160–180 nm are referred to as LBH-long (LBH-L). The LBH band has been an important imaging target of several satellites, including the wide-field auroral imager (WAI)/FY-3D [1], WAI/FY-3H, WIC/IMAGE [2], and UVI/Polar [3]. Besides near ultraviolet and visible lines, there are also strong lines of 121.6 nm (H), 130.4 nm, and 135.6 nm (O) in the aurora, which destroy the imaging quality of the LBH band. Hence, out-of-band suppression must be taken into account in the design of optical systems. UVI/Polar used three reflective mirrors and a transmissive filter to image LBH-S and LBH-L, respectively. The reflective mirror was composed of 35 layers of periodic LaF_3/MgF_2 and a Pyrex substrate; the reflectances were about 25%, 30%, 58% at 121.6 nm, 130.4 nm, and 135.6 nm, respectively, and out-of-band reflection suppression of the periodic LaF_3/MgF_2 multilayer was poor. The out-of-band reflection suppression of their optical system was mainly achieved by transmissive filters [3]. WIC/IMAGE selected an inverted Cassegrain optical system to image the LBH band. They used two broadband reflective mirrors, and these mirrors also provided near ultraviolet and visible suppression. Unfortunately, they did not give the structure of the mirrors; the reflectances were 40%, 15%, and 40% at 121.6 nm, 130.4 nm, and 135.6 nm, respectively, and out-of-band reflection suppression of their broadband mirror was not good [2]. WAI/FY-3D and WAI/FY-3H of China both chose four reflective mirrors. Besides a BaF_2 filter, no other filters were used. Hence, reflective mirrors must provide strong out-of-band suppression. WAI/FY-3D detected LBH bands, and a 22-layer non-periodic LaF_3/MgF_2 broadband mirror was used [1,4]. Bandwidth extended technology was utilized to achieve a broad band of 40 nm. The average reflectance was about 10% at 185–220 nm, but was still too high. WAI/FY-3H detects LBH-S and LBH-L bands, and stricter out-of-band suppression is proposed.

Because of the relatively low absorption and good stability, a LaF_3/MgF_2 multilayer has been widely used in the far ultraviolet (FUV) region, such as 193 nm lithography [5], 157 nm laser lithography [6], and astronomical exploration [4]. A variety of periodic LaF_3/MgF_2 multilayers have been designed and fabricated and their optical properties extensively studied [7–21]. The Zukic group utilized the natural absorption of one of the film materials to block the transmission at shorter wavelengths in a Fabry–Perot filter and chose a reflection filter to reject the transmission of the Fabry–Perot filter at the longer wavelength. The average transmittance was smaller than 0.1% in the longer wavelength, the transmittance was smaller than 0.1% in the shorter wavelength, and the two filters had a bandwidth of smaller than 5 nm and a peak transmittance of higher than 25% [7]. Although a non-periodic multilayer was widely used to design a reflective filter with good out-of-band suppression,

no such LaF_3/MgF_2 multilayer has been reported. Fluoride material films deposited by boat and electron-beam evaporation exhibited tensile stress [13,16,17]. Strategies such as reducing substrate temperature and introducing a third material as a stress compensation layer were proposed to enhance the laser-induced-damage threshold [9,11,12,20]. Optical constants of LaF_3 and MgF_2 were studied as a function of film deposition conditions [8,14]. MgF_2 and LaF_3 films can be deposited by ion-beam sputtering or boat and electron-beam evaporation; those deposited by ion-beam sputtering demonstrated the best homogeneity and lowest surface roughness value of about 0.7 nm, as well as high compressive stress [18,19,21]. Because the porous column structure of fluoride materials is prone to absorb the water, they exhibit a reflectance shift to longer wavelengths over time [20]. If LaF_3/MgF_2 is deposited on a fused silica substrate, it will easily crack, resulting from the large difference of thermal expansion coefficients (TECs) between the substrate and the film. The crack phenomenon can be alleviated if one chooses a fluoride substrate, and reduces substrate heating temperature and layer numbers [4,22]. AlF_3 was used to replace MgF_2, and better optical properties were achieved, but more attention should be paid to stability in the long term [23]. To date, due to its good application heritage, the LaF_3/MgF_2 multilayer is still the first choice in astronomical exploration.

Based on the requirements of WAI/FY-3H, non-periodic LaF_3/MgF_2 multilayer mirrors were designed and fabricated, with working wave bands of 140–160 nm and 160–180 nm, respectively.

2. DESIGN

The designer of the optical system gave us design targets or requirements for mirrors, including average reflectance in the working wavelength, and reflectance suppression (RS) ratio between out-of-band and in-band. The requirements are given in Table 1, derived from overall consideration of the intensity of emission lines for the aurora, quantum efficiency of the microchannel plate (MCP) detector, and transmittance of the BaF_2 filter. Details can be found in the literature.

A. Optical Constants

The optical constants of LaF_3 and MgF_2 were derived from the characterization of reflectance of a single layer by OptiLayer software [24]. The single layer of LaF_3 or MgF_2 was fabricated under the same coating process as multilayer mirrors. The nominal thickness of the single layer was 130 nm, incident angles were 10° and 20°, respectively, and the substrate was Zerodur. Figure 1 shows the fittings of experimental reflectance curves for LaF_3 (a), (b) and MgF_2 (c), (d). The goodness of fit was 1.03 and 0.20, respectively. The wavelength ranged from 120 nm to 220 nm, and the inhomogeneities were −24.3% and 3.9%, respectively. The work of Lin demonstrated that the inhomogeneity of LaF_3 can be enhanced to −2.14% at a substrate heating temperature of 400° [25], and the inhomogeneity was −12.85% at 250°. The substrate heating temperature was 170° in our experiment; hence, the inhomogeneity of LaF_3 was lower than their samples. The fitting was not as good from 120 nm to 130 nm for LaF_3, and this may result from its high inhomogeneity. The fitting for MgF_2 was excellent. Figure 2 demonstrates the optical constants of LaF_3 (a) and MgF_2 (b) in the range from 120 nm to 220 nm, respectively.

B. Match Method Design

A quarter-wave (QW) periodic stack is a basic dielectric reflecting structure; by increasing the period number, the reflectance at the working wave band can be significantly enhanced, and transition from the reflecting to transmitting zone becomes sharper. The shortcoming is that it has pronounced sideband ripples and must be suppressed in a filter application. Sideband ripples result from the mismatch between the QW stack and surrounding media (air and substrate). A symmetrical period can be mathematically treated as a single equivalent layer with an equivalent phase thickness and equivalent admittance (Herpin index), allowing many advantages and convenience for the analysis and design of filters [26]. Our match design idea is that we choose a symmetrical periodic multilayer with better matching with surrounding media as the main structure of the notch filter, add a special layer to match with residual surrounding media, and finally refine the multilayer by Optilayer software.

We used symmetrical periodic multilayers of $(0.5LH0.5L)^m$ and $(0.5HL0.5H)^n$ to design reflective stacks [26]: (0.5LH0.5L) and (0.5HL0.5H) are basic symmetrical periods, L denotes low-index material with a QW optical thickness, H denotes high-index material with a QW optical thickness, and m and n are periodic numbers. The working wavelengths were 140–160 nm and 160–180 nm, respectively. The substrate was Zerodur, and incident angle was 33.5°; this angle was the incident angle of one of the mirrors in our optical system.

Figure 3 reveals the calculated equivalent parameters of $(0.5LH0.5L)^m$ and $(0.5HL0.5H)^n$. For comparison, the

Table 1. Requirements and Theoretical and Experimental Results for the Mirrors

	Reflectance at Working Wavelength	Reflectance/RS at 121.6	Reflectance/RS at 130.4	Reflectance/RS at 135.6	Reflectance/RS at 160–180 (LBH-S) or at 140–160 (LBH-L)	Reflectance RS at 180–220
LBH-S (requirement)	>35.00%	<0.150	<0.100	<0.250	<0.200	<0.125
LBH-S (theory)	39.28%	0.61%/0.016	0.34%/0.009	0.31%/0.008	2.4%/0.061	1.55%/0.039
LBH-S (experiment)	42.87%	6.09%/0.142	2.12%/0.049	5.52%/0.129	4.65%/0.108	1.69%/0.039
LBH-L (requirement)	>40.00%	<0.15	<0.100	<0.167	<0.200	<0.125
LBH-L (theory)	43.22%	0.42%/0.010	0.57%/0.013	0.90%/0.021	4.3%/0.099	3.7%/0.086
LBH-L (experiment)	48.53%	4.81%/0.099	2.71%/0.056	1.60%/0.033	6.74%/0.139	4.35%/0.090

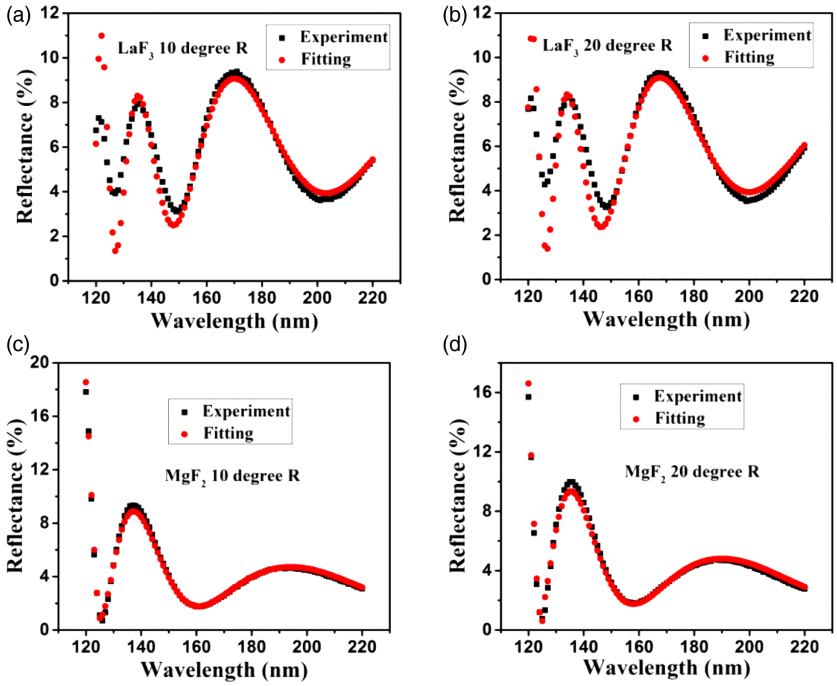

Fig. 1. Fittings of experimental reflectance curves for LaF_3 (a) 10° and (b) 20° and for MgF_2 (c) 10° and (d) 20°.

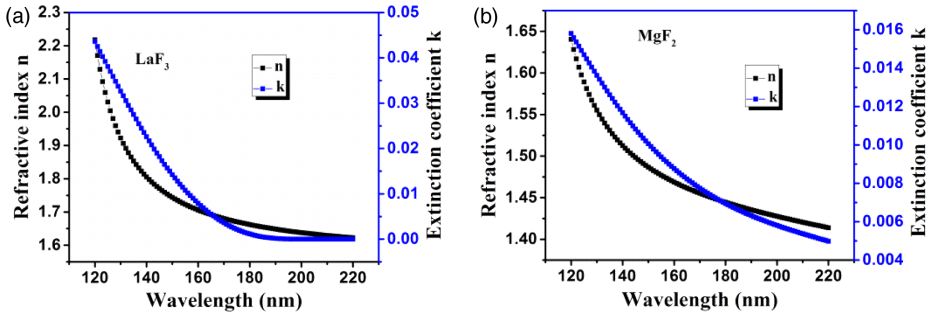

Fig. 2. Optical constants of (a) LaF_3 and (b) MgF_2.

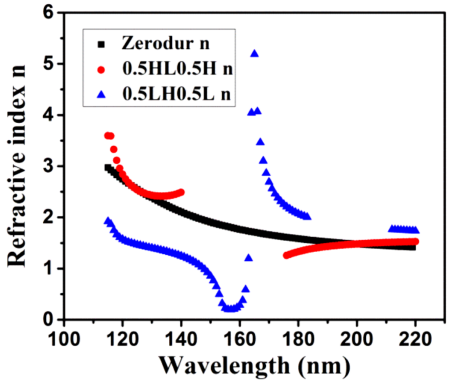

Fig. 3. Calculated equivalent parameters of $(0.5LH0.5L)^m$ and $(0.5HL0.5H)^n$.

refractive index of the Zerodur substrate is also provided. The refractive index of (0.5HL0.5H) demonstrated a better match with that of the Zerodur substrate than (0.5LH0.5L) out of 140–180 nm. Hence, we chose the stack of $(0.5HL0.5H)^7$ as the main structure of the mirror.

Figure 4 gives the optimization design of LBH-S (a) and LBH-L (b) multilayers. There was high reflectance at 120–137 nm for the initial design of $(0.5HL0.5H)^7$. This resulted from the mismatch of refractive index between $(0.5HL0.5H)^7$ and air. The low-refractive-index material of MgF_2 was the best choice to solve this problem. Because the wavelength of 120 nm was the shortest target for RS, and average working wavelengths were 150 nm and 170 nm, the thicknesses of the antireflection layer (matching layer) were determined to be 0.8L (120/150) for LBH-S and 0.7L (120/170) for LBH-L. Hence, 0.8L and 0.7L were added into LBH-S and LBH-L multilayers, respectively. The reflectances at 120–137 nm were effectively suppressed, and the drawback was that there was little reflectance increase in the longer wavelength, especially 175 nm for the LBH-S mirror and 185 nm and 200 nm for the LBH-L mirror. The Refine function of OptiLayer software [25] was used to further optimize the multilayers; tolerances were set to 0.01 for 121.6 nm, 130.4 nm, and 135.6 nm, and

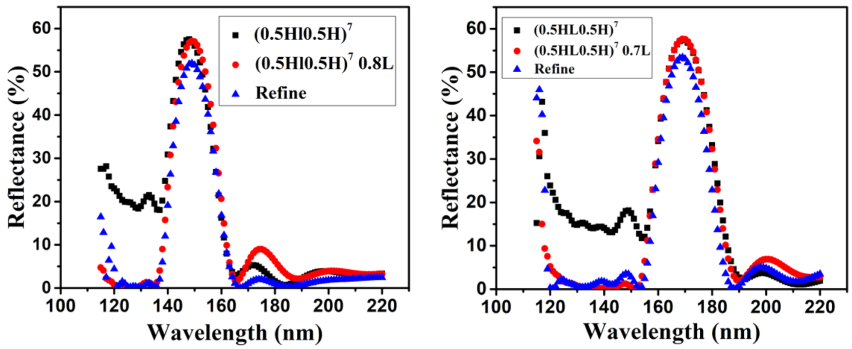

Fig. 4. Optimization design of (a) LBH-S multilayer and (b) LBH-L multilayer.

others were set to one. Finally, good optical performance was achieved. For the LBH-S mirror, the average reflectance was 39.28%. Reflectances were 0.61%, 0.34%, 0.31%, 2.4%, and 1.55% at 121.6 nm, 130.4 nm, 135.6 nm, 161–180 nm, and 181–220 nm, respectively. For the LBH-L mirror, the average reflectance was 43.22%. Reflectances were 0.42%, 0.57%, 0.90%, 4.3%, and 3.7% at 121.6 nm, 130.4 nm, 135.6 nm, 140–159 nm, and 181–220 nm, respectively. All these data are summarized in Table 1. The layer number was 16, and the total thicknesses of LBH-S and LBH-L nm mirrors were 353 nm and 414 nm, respectively.

C. Deep Search Design

Stimulated by the rapid development of machine-learning and deep search optimization methods [27–32], we also used the deep search method of Optilayer software to design the mirrors. A 17-layer solution to our LBH-L mirror was found by the deep search gradual evolution method without any stated design in a completely automatic mode [32]. Figure 5 demonstrates the design results of the deep search. Compared with our match design method, the deep search design gave better results: higher peak reflectance, and better RS at 121.6 nm, 130.4 nm, and 135.6 nm [Fig. 5(a)]. On the contrary, this multilayer had 17 layers, and the first layer was MgF_2. Deep search was indeed a fast, effective design method, and it demonstrated a noticeable advantage. However, the multilayer designed by deep search had a total thickness of 528.5 nm, which was 114.5 nm thicker than that obtained by our match design method. This would lead to cracking of thin films, resulting from thermal stress of thicker fluoride films. Hence, we reduced the layer number from 17 to 15, and redesigned the multilayer. Unfortunately, in a 15-layer multilayer, the total thickness was still 525.5 nm, and it exhibited worse RS at 121.6 nm, 130.4 nm, and 135.6 nm [Fig. 5(b)]. Figure 6 gives the thickness distribution in multilayers designed by the match method (16 layers) and deep search method (15 layers and 17 layers). Most of the layer thickness was in the range from 10 nm to 45 nm, but the thickness of the 16th layer was 65 nm in the 17-layer deep search design; the thicknesses of the sixth and 14th layers were 80 nm and 65 nm, respectively, in the 15-layer deep search design. Deep search was prone to give some extreme thicker layer in its design. Large film thickness deviation may lead to some difference in refractive index and inhomogeneity. For optical thin film deposition in the FUV region, only a quartz monitor is used to control film thickness. A quartz monitor can control only physical thickness (d), not optical thickness (nd; n is the refractive index of films), as optical monitoring can. A large film thickness brings large errors in thickness control. Thus, taking into account practical fabrication, we discarded the multilayer structure obtained by the deep search method.

3. FABRICATION

LaF_3 and MgF_2 were put in a molybdenum boat and deposited by the resistive thermal evaporation method. The deposition rate was 0.2 nm/s, and the substrate was the Zerodur. The deposition rates were controlled by a quartz monitor. The base pressure was 2.5×10^{-4} Pa, and the substrate heating temperature was 170°. The deposition parameters of the layer number, the total thickness, and the substrate heating temperature were

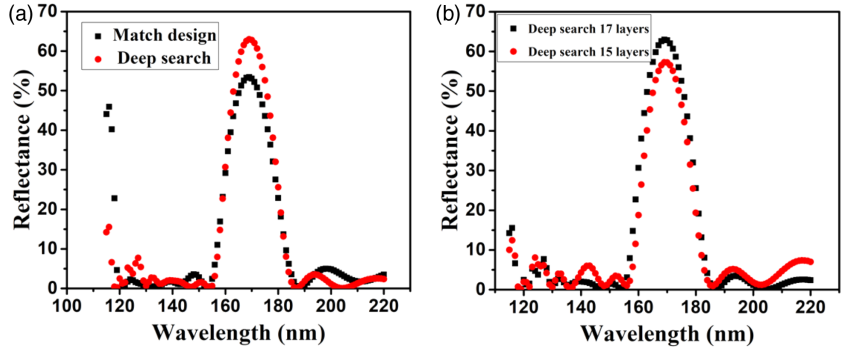

Fig. 5. Design results of the deep search: comparison of the (a) match design and (b) deep search design with 15 layers and 17 layers.

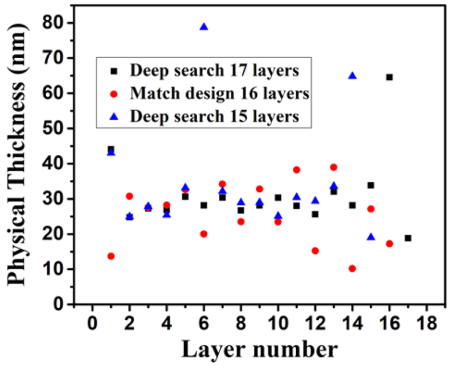

Fig. 6. Thickness distributions in multilayer: 16 layers in the match design, 15 layers and 17 layers in the deep search design.

determined by the criterion that no cracks were observed by the white interferometer [4].

A. Reflectance

The reflectance of the mirror was measured by a McPherson VUVaS2000 ultraviolet spectrophotometer with a step of 1 nm, and the base pressure was 4×10^{-3} Pa.

Figure 7 gives the experimental results of our fabricated mirrors. The LBH-L mirror exhibited better agreement between theoretical calculation and experiment than LBH-S. For the LBH-S mirror, the average reflectance was 42.87%. Reflectances were 6.09%, 2.12%, 5.52%, 4.65%, and 1.69% at 121.6 nm, 130.4 nm, 135.6 nm, 161–180 nm, and 181–220 nm, respectively. For the LBH-L mirror, the average reflectance was 48.53%. Reflectances were 4.81%, 2.71%, 1.60%, 6.74%, and 4.35% at 121.6 nm, 130.4 nm, 135.6 nm, 140–159 nm, and 181–220 nm, respectively. As shown in Table 1, the test results of the fabricated mirrors demonstrated a small deviation from the design, especially in terms of the out-of-band inhibition capability. This may result from the thickness dependence of the optical constants [5], larger inhomogeneity of LaF_3, thickness control errors, or test errors. We utilized a single layer coating with a thickness of 130 nm to derive the optical constants, and its thickness was quite larger than the thickness of each layer in the multilayer. Even though the single layer coating and multilayer were deposited under the same deposition process, the optical constants may have little difference due to its thickness dependence [5]. In FUV coating deposition, only a quartz monitor was used to control the physical thickness rather than optical thickness, which an optical monitor can control, and this may introduce some thickness errors. The ultraviolet spectrophotometer used a deuterium lamp as a light source, and the intensity of its emission lines at 115–136 nm is weak. Hence, the accuracy of measured reflectance may be not good.

B. Stress

It is well known that high substrate temperatures (200°–300°C) during deposition results in lower intrinsic stress and higher thermal stress for MgF_2 film [5,13,16,17]. Thus, our fabricated LaF_3/MgF_2 ML has strong thermal stress. As shown in Eq. (1), the total stress of the LaF_3/MgF_2 multilayer includes thermal stress and intrinsic stress [13,16,17,22]. Thermal stress can be calculated by Eq. (2), where E is the Young's modulus, ν is the Poisson ratio of the coating, α_{sub} and α_{film} are the TECs of the substrate and film, respectively, T is the room temperature, and T_d is the substrate heating temperature during deposition [13,16,17,22].

Traditionally, as shown in Fig. 8, the film stress brings about a curvature change on the substrate. The tensile stress makes the substrate surface become concave, and the large tensile stress generates cracks [33]. The traditional stress can be calculated by Eq. (3) (Stoney equation), where d_s and d_f are the thicknesses of the substrate and film, and R_d and R_0 are substrate radii before (R_0) and after (R_d) film deposition, respectively [13,16,17,22]. It was found that the film cracked when the substrate heating temperature was 230°C during deposition. Although no crack occurred for the film, the surface figure of the substrate changed significantly when the substrate heating temperature was 180°–220°C during deposition. Figure 9 gives the stress of films when the substrate heating temperature is 170°–220°C during deposition. The stress was calculated by Eq. (3), the parameters were cited from Refs. [17,34], and the stress was the sum of LaF_3 and MgF_2. Films deposited at 170°C had a tensile stress of 536 MPa, the surface figure had a small variance after deposition, and optical performance was stable after three months. The equations are as follows:

$$\sigma_{total} = \sigma_{therm} + \sigma_{intr}, \tag{1}$$

$$\sigma_{therm} = \left(\frac{E}{1-\vartheta}\right)_{film} (\alpha_{sub} - \alpha_{film})\,(T - T_d)\,, \tag{2}$$

$$\sigma_{total} = \frac{E}{1-\vartheta}\frac{d_s^2}{6d_f}\left(\frac{1}{R_d} - \frac{1}{R_0}\right). \tag{3}$$

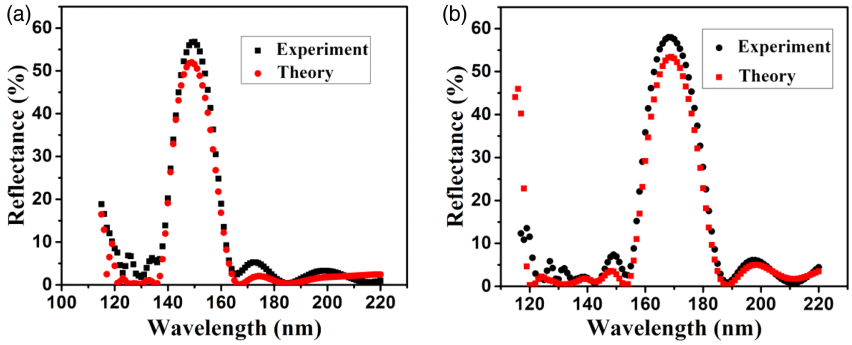

Fig. 7. Experimental results of our fabricated multilayers: (a) LBH-S and (b) LBH-L.

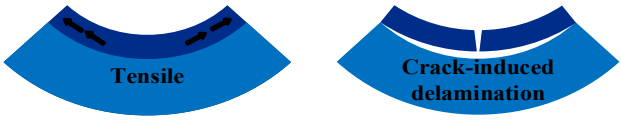

Fig. 8. Illustration of the effect of a thin film with tensile stress on the substrate bending [33].

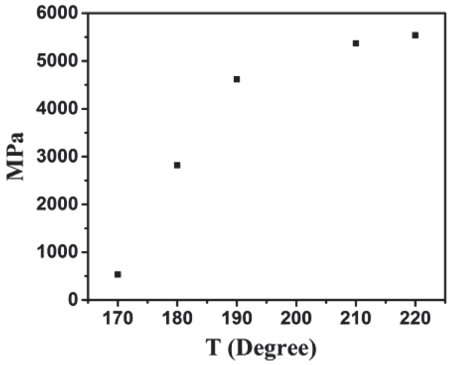

Fig. 9. Stress of films when the substrate heating temperature is 170°–220°C during deposition.

4. CONCLUSIONS

To meet the requirement of WAI/FY-3H, we designed and fabricated a non-periodic LaF_3/MgF_2 multilayer. The working wavelengths were 140–160 nm and 160–180 nm, respectively. The optical constants of LaF_3 and MgF_2 were derived by the characterization of the reflectance at two incident angles for the single layer.

Deep search was used to solve our problem, and it exhibited a noticeable advantage. The multilayer designed by this method showed excellent optical performance. However, it needed thicker multilayers. This led to cracks in the film, resulting from the thermal stress of fluoride film. Thus, we proposed the match design method to design the multilayer. Due to its better match, the refractive index of the Zerodur substrate $(0.5HL0.5H)^7$ was selected as the main structure of the multilayer, MgF_2 was used to match the difference of the refractive index between the unit of (0.5HL0.5H) and air, and the Refine function of Optilayer software was used to further optimize the multilayer. The fabricated mirrors exhibited excellent optical performances, as used in WAI/FY-3H.

If a single layer LaF_3 coating with different thicknesses is deposited, optical constants of LaF_3 may be more precisely characterized. If a new deuterium lamp is used in the ultraviolet spectrophotometer, measurement accuracy may be enhanced. All of these efforts may contribute to reduce the disagreement between experiment results and design. Due to a lower tensile stress of AlF_3 compared with MgF_2, AlF_3/LaF_3 is another promising potential material pair candidate. More layers can be used in this multilayer, the deep search method may be effectively used to design this thicker multilayer, and better optical performance may be achieved. However, space adaptability of the AlF_3/LaF_3 coating should be seriously considered.

Funding. National Natural Science Foundation of China (12273040); Joint Fund of Astronomy (U2031122); Chinese Academy of Sciences.

Acknowledgment. We thank Professor Alexander Tikhonravov from Moscow State University for fruitful discussions of characterization of the optical constant of MgF_2 films.

Disclosures. The authors declare no conflicts of interest.

Data availability. Data underlying the results presented in this paper are not publicly available at this time but may be obtained from the authors upon reasonable request.

REFERENCES

1. X. Zhang, B. Chen, F. He, *et al.*, "Wide-field auroral imager onboard the Fengyun satellite," Light Sci. Appl. **8**, 47 (2019).
2. S. B. Mende, H. Heetderks, H. U. Frey, M. Lampton, S. P. Geller, R. Abiad, O. H. W. Siegmund, A. S. Tremsin, J. Spann, H. Dougani, S. A. Fuselier, A. L. Magoncelli, M. B. Bumala, S. Murphree, and T. Trondsen, "Far ultraviolet imaging from the image spacecraft. 2. Wideband FUV imaging," Space Sci. Rev. **91**, 271–285 (2000).
3. M. R. Torr, D. G. Torr, M. Zukic, R. B. Johnson, J. Ajello, P. Banks, K. Clark, K. Cole, C. Keffer, G. Parks, B. Tsuratani, and J. Spann, "A far ultraviolet imager for the International Solar-Terrestrial Physics Mission," Space Sci. Rev. **71**, 329–383 (1995).
4. X. Wang, B. Chen, and L. Yao, "Design and fabrication of far-ultraviolet reflective broadband filter based on dielectric materials," Appl. Spectrosc. **72**, 943–946 (2018).
5. C. Liu, M. Kong, and B. Li, "Performance optimization of 193 nm antireflective coatings with wide incident angle ranges on strongly curved spherical substrates," Opt. Express **26**, 19524–19533 (2018).
6. S. Niisaka, T. Saito, J. Saito, A. Tanaka, A. Matsumoto, M. Otani, R. Biro, C. Ouchi, M. Hasegawa, Y. Suzuki, and K. Sone, "Development of optical coatings for 157-nm lithography. I. Coating materials," Appl. Opt. **41**, 3242–3247 (2022).
7. M. Zukic, D. G. Torr, J. F. Spann, and M. R. Torr, "Vacuum ultraviolet thin films 2: vacuum ultraviolet all-dielectric narrowband filters," Appl. Opt. **29**, 4293–4302 (1990).
8. O. R. Wood, H. G. Craighead, J. E. Sweeney, and P. J. Maloney, "Vacuum ultraviolet loss in magnesium fluoride films," Appl. Opt. **23**, 3644–3649 (1984).
9. H. Bernitzki, H. Lauth, R. Thielsch, H. Blaschke, N. Kaiser, and K. R. Mann, "Current status of radiation resistance of dielectric mirrors in the DUV," Proc. SPIE **3578**, 105–116 (1999).
10. R. Thielsch, "Optical coatings for the DUV/VUV," in *Optical Interference Coatings*, N. Kaiser and H. K. Pulker, eds. (Springer, 2003), pp. 257–277.
11. J. E. Rudisill, A. Dupparre, and S. Schroeder, "Determination of scattering losses in ArF excimer laser all-dielectric mirrors for 193 nm microlithography application," Proc. SPIE **5647**, 9–22 (2005).
12. S. Günster, D. Ristau, A. Gatto, N. Kaiser, M. Trovó, and M. Danailov, "Storage ring free-electron lasing at 176 nm-dielectric mirror development for vacuum ultraviolet free-electron lasers," Appl. Opt. **45**, 5866–5870 (2006).
13. G. H. Liu, Q. L. Xiao, Y. X. Jin, W. L. Zhang, H. B. He, and Z. X. Fan, "Mechanical stress in 355 nm LaF_3/MgF_2 high reflectors with various layer-pair number and methods for reduction," Vacuum **84**, 778–781 (2010).
14. L. Rodríguez-de Marcos, J. I. Larruquert, J. A. Méndez, and J. A. Aznárez, "Multilayers and optical constants of various fluorides in the far UV," Proc. SPIE **9627**, 96270B (2015).
15. L. V. R. De Marcos, J. I. Larruquert, J. A. Méndez, N. Gutiérrez-Luna, L. Espinosa-Yáñez, C. Honrado-Benítez, J. Chavero-Royán, and B. Perea-Abarca, "Optimization of MgF_2–deposition temperature for far UV Al mirrors," Opt. Express **26**, 9363–9372 (2018).
16. J. Ullmann, H.-G. Keck, R. Thielsch, H. Uhlig, and N. Kaiser, "Mechanical stress in fluoride coatings," Proc. SPIE **3738**, 136–147 (1999).
17. R. Thielsch, J. Heber, H. Uhlig, and N. Kaiser, "Development of mechanical stress in fluoride multilayers for UV applications," Proc. SPIE **5250**, 127–136 (2004).

18. D. Ristau, S. Günster, S. Bosch, A. Duparré, E. Masetti, J. Ferré-Borrull, G. Kiriakidis, F. Peiró, E. Quesnel, and A. Tikhonravov, "Ultraviolet optical and microstructural properties of MgF_2 and LaF_3 coatings deposited by ion-beam sputtering and boat and electron-beam evaporation," Appl. Opt. **41**, 3196–3204 (2002).
19. S. Schröder, H. Uhlig, A. Duparré, N. Kaiser, F. Angewandte, and D. Jena, "Nanostructure and optical properties of fluoride films for high-quality DUV/VUV optical components," Proc. SPIE **5963**, 59630R (2005).
20. D. R. J. Kolbe, H. Kelsser, T. Hofmann, F. Meyer, and H. Schink, "Optical properties and damage thresholds of dielectric UV/VUV-coatings deposited by conventional evaporation, IAD and IBS," Proc. SPIE **1624**, 221–235 (1992).
21. L. Dumas, E. Quesnel, J.-Y. Robic, and Y. Pauleau, "Characterization of magnesium fluoride thin films deposited by direct electron beam evaporation," J. Vac. Sci. Technol. A **18**, 465–469 (2000).
22. P. López-Reyes, B. Perea-Abarca, C. Honrado-Benítez, N. Gutiérrez-Luna, A. Ríos-Fernández, L. V. Rodríguez-de Marcos, and J. I. Larruquert, "Optimization of the deposition parameters of MgF_2/LaF_2 narrowband reflective FUV multilayers," Opt. Mater. Express **11**, 1678–1691 (2021).
23. P. López-Reyes, C. Honrado-Benítez, N. Gutiérrez-Luna, A. Ríos-Fernández, L. V. Rodríguez-de Marcos, and J. I. Larruquert, "Far-UV reflectance and stress of narrowband AlF_3/LaF_3 multilayers," Opt. Mater. Express **12**, 489–502 (2022).
24. A. V. Tikhonravov and M. K. Trubetskov, "OptiLayer thin film software," http://www.optilayer.com.
25. D. Lin, C. Guo, and B. Li, "Refractive index inhomogeneity of LaF_3 film at deep ultraviolet wavelength," Chin. Opt. Lett. **11**, S10602 (2013).
26. H. A. Macleod, *Thin-Film Optical Filters*, 4th ed. (CRC Press/Taylor & Francis, 2010).
27. Y. LeCun, Y. Bengio, and G. Hinton, "Deep learning," Nature **521**, 436–444 (2015).
28. M. Fouchier, M. Zerrad, M. Lequime, and C. Amra, "Design of multilayer optical thin-films based on light scattering properties and using deep neural networks," Opt. Express **29**, 32627–32638 (2021).
29. I. Sajedian, H. Lee, and J. Rho, "Design of high transmission color filters for solar cells directed by deep Q-learning," Sol. Energy **195**, 670–676 (2020).
30. A. Jiang, Y. Osamu, and L. Chen, "Multilayer optical thin film design with deep Q learning," Sci. Rep. **10**, 12780 (2020).
31. V. T. Tran, H. V. Mai, H. M. Nguyen, D. C. Duong, V. H. Vu, N. N. Hoang, M. V. Nguyen, T. A. Mai, H. D. Tong, H. Q. Nguyen, Q. Nguyen, and T. Nguyen-Tran, "Machine-learning reinforcement for optimizing multilayered thin films: applications in designing broadband antireflection coatings," Appl. Opt. **61**, 3328–3336 (2022).
32. M. Trubetskov, "Deep search methods for multilayer coating design," Appl. Opt. **59**, A75–A82 (2020).
33. S. Massahi, L. M. Vu, D. D. M. Ferreira, F. E. Christensen, N. Gellert, P. L. Henriksen, S. Svendsen, A. S'Jegers, M. Collon, B. Landgraf, D. Girou, A. Thete, B. Shortt, I. Ferreira, and M. Bavdaz, "Balancing of residual stress in thin film iridium by utilizing chromium as an underlayer," Proc. SPIE **11444**, 114444N (2020).
34. Z. Lv, C. Cheng, Y. Cheng, X. Chen, and G. Ji, "Elastic, thermodynamic and electronic properties of LaF_3 under pressure from first principles," Comput. Mater. Sci. **89**, 57–64 (2014).